*Progress In Electromagnetics Research C, Vol. 120, 223–241, 2022*

# Optimal Design of a Circularly Polarized Antenna for LTE Bands 42/43 Applications

**Saja A. Gheni and Dhirgham K. Naji***

**Abstract**—In this paper, an optimized circularly polarized (CP) antenna is proposed for operating in the LTE bands 42/43 applications. This CP antenna comprises three sections, the meander-line and L-shaped strip structures modeled on the front side of a Roger 3003 substrate, and on the back side a rotated H-shaped ground plane is printed. In order to further increase the antenna common bandwidth (CBW), that is the voltage standing wave ratio bandwidth (VRBW) and axial ratio bandwidth (ARBW), an offset-fed line on the front side and a shorting pin are used. A feasible solution of the optimized CP antenna with compact size is achieved by applying an optimization design methodology with a fitness function that takes into account the antenna performance parameters, CBW, or both the VRBW and ARBW in addition to the realized gain (RG). Two programs are operating in synchronous fashion for finding the optimal geometric antenna parameters, a particle swarm optimization (PSO) for implementing the fitness function in MATLAB and a CST MWS simulator tool for extracting the antenna performance parameters. The optimized antennas without and with shorting pin are obtained with a broadest CBW and feature of CP operation and an acceptable RG across the desired LTE 42 (3.4–3.6 GHz) and LTE 42/43 (3.4–3.8 GHz) band, respectively. The proposed two designed antennas, with and without shorting pin, are fabricated, and the measured results are in good agreement with the simulated ones. From measured results, a $-10$ B-$S_{11}$ impedance bandwidth (IBW) of 220 MHz (3.38–3.60 GHz) and 460 MHz (3.37–3.83 GHz), a 3-dB ARBW of 200 MHz (3.4–3.6 GHz) and 390 MHz (3.42–3.81 GHz) with respective maximum RG of 2.26 and 2.39 dBic are exhibited by the antennas without and with pin, respectively. The obtained 3-dB ARBWs and $-10$-dB IBWs make the proposed antennas entirely cover the LTE 42 or LTE 42/43 frequency bands.

## 1. INTRODUCTION

With the rapid development and growth of wireless communication and the fifth generation (5G), it is critical to meet the growing network demands. It is expected that 5G will offer significantly higher throughput, especially LTE (long-term evolution). This will lead to activating new business models, applications, and industries, as well as improving life quality through exceptional use cases that require communications with high data-rate, low latency, and massive connectivity for applications like autonomous vehicles and Internet of Things (IoT) [1, 2]. In comparison to linear polarization (LP), circular polarization (CP) radiation pattern has better performance, mobility, and orientation freedom, as well as lower multipath interference and fading. CP antennas are broadly utilized in many communication systems in view of the advantages of keeping away from polarization arrangement between the transmitter and receiver, and reducing multi-path effects. In general, an ideal circular polarization is produced by two symmetrical electric field vectors with equivalent amplitudes and a 90° phase difference (PD) [3]. CP antenna enjoys various significant benefits contrasted with antennas

*Received 14 April 2022, Accepted 23 May 2022, Scheduled 7 June 2022*

* Corresponding author: Dhirgham K. Naji (dhrgham.kamal@gmail.com).
The authors are with the Department of Electronic and Communications Engineering, College of Engineering, Al-Nahrain University, Baghdad, Iraq.

utilizing linear polarizations and is turning into a critical innovation for different wireless systems such as satellite communications, mobile communications, and Worldwide Interoperability for Microwave Access (WiMAX) [4–9].

Different types of structures have been proposed in open literature for generating CP waves. Some of these types are crossed dipoles [10], arrays of parasitic elements [11], and antennas having patches with conventional geometric shapes, square, circle, and ellipse, are used for producing circular polarization radiation [12, 13]. To extend both the −10-dB impedance bandwidth (IBW) and 3-dB axial ratio bandwidth (ARBW), that is the common bandwidth (CBW), many techniques have been presented [14–18]. In [14], a design method based on edges as the form of steps has been implemented for a CP crossed dipole antenna with broadband CBW. The broad CP radiation of the patch antennas is obtained by introducing shorting pins [15], nonuniform metasurface [16], parasitic elements [17], and symmetrical slots [18].

The aforementioned antennas are designed either by a trial-and-error procedure and parameters sweeping or based on experience and ingenuity of the antenna designer. Modern antennas must fulfill different electrical and field characteristics intended for them. The optimal antenna design involves improving its performance by fine-tuning geometry parameters within their allowed prescribed ranges. Therefore, a scalar objective (fitness) function for measuring the quality of enhancement in the performance is quite necessary by implementing EM-based tuning of geometric antenna parameters. In the case of multi-objectives, one of them may be selected as the primary objective while the others are considered as secondary objectives controlled by suitably defined constraints [19–21]. Recently, a novel algorithm for design optimization of a CP antenna structure is presented in [22]. This algorithm is formulated as an optimization problem to find the best geometric antenna parameters that satisfy the design requirements including best matching design ($S_{11}$), realized gain (RG) maximization, axial ratio (AR) improvement, and antenna size reduction. Also, in [23], a CP antenna with a miniaturized size and broadband capabilities is designed, and it is analyzed by the Genetic Algorithm (GA) optimizer to find the optimum parameters for the cost function that takes into account $S_{11}$, $AR$, and $RG$ in the forward direction, at discrete frequency points.

In this paper, optimal two antennas (one without and the other with shorting pin) with feature of CP radiation for (the LTE 42 and LTE 42/43 band) applications are presented. These two antennas are obtained after a series of modifications have been done for the conventional rectangular microstrip antenna (RMA) to improve its performance across the desired LTE bands, including CBW and RG. An optimization methodology based on a CST Microwave Studio is used as an EM simulator for analysis and extracting the antenna performance parameters, and the Particle Swarm Optimization (PSO) implemented in MATLAB, as an optimizer algorithm, to find the optimum parameters of the fitness function. A detailed description of the design methodology and its application for obtaining the two optimal antenna structures as well as their important performance parameters are given. After that, the current distribution and radiation patterns of the two proposed antennas at their frequency band of interest are provided to validate the CP radiation. Finally, the antennas are fabricated and measured for validating the simulated results.

## 2. A DESIGN PROCEDURE OF THE PROPOSED ANTENNAS

The design procedure of the two proposed circularly polarized (CP) antennas are presented in this section. Four iterations or steps for five antennas, Ant0 through Ant4, are shown in Fig. 1 with modification between steps. Fig. 2 shows the detailed configurations of the optimal CP antennas, with and without shorting pin, denoted as Ant3 and Ant4, respectively. Table 1 summarizes the optimal dimension parameters of the antennas. The reflection coefficient, $s_{11}$, and axial ratio (in $+z$ direction) against frequency are depicted in Figs. 3 and 4, respectively. All the five designed antennas are placed on the upper side of a Roger 3003 substrate of an overall size $W_{sub}\times L_{sub}\times h_{sub}$ (dielectric constant $\varepsilon_r$= 3, loss tangent $\tan\delta = 0.001$, and a height of $h_{sub}$= 1.6 mm). These four design steps are described in detail as below.

**Step 1:** As shown in Fig. 1(a), Ant0 represents a conventional inset-fed rectangular microstrip antenna (RMA). For this antenna, the patch width $W_p$ and length $L_p$ represent the main geometric antenna parameters that depend on the specification information including dielectric constant $\varepsilon_r$,

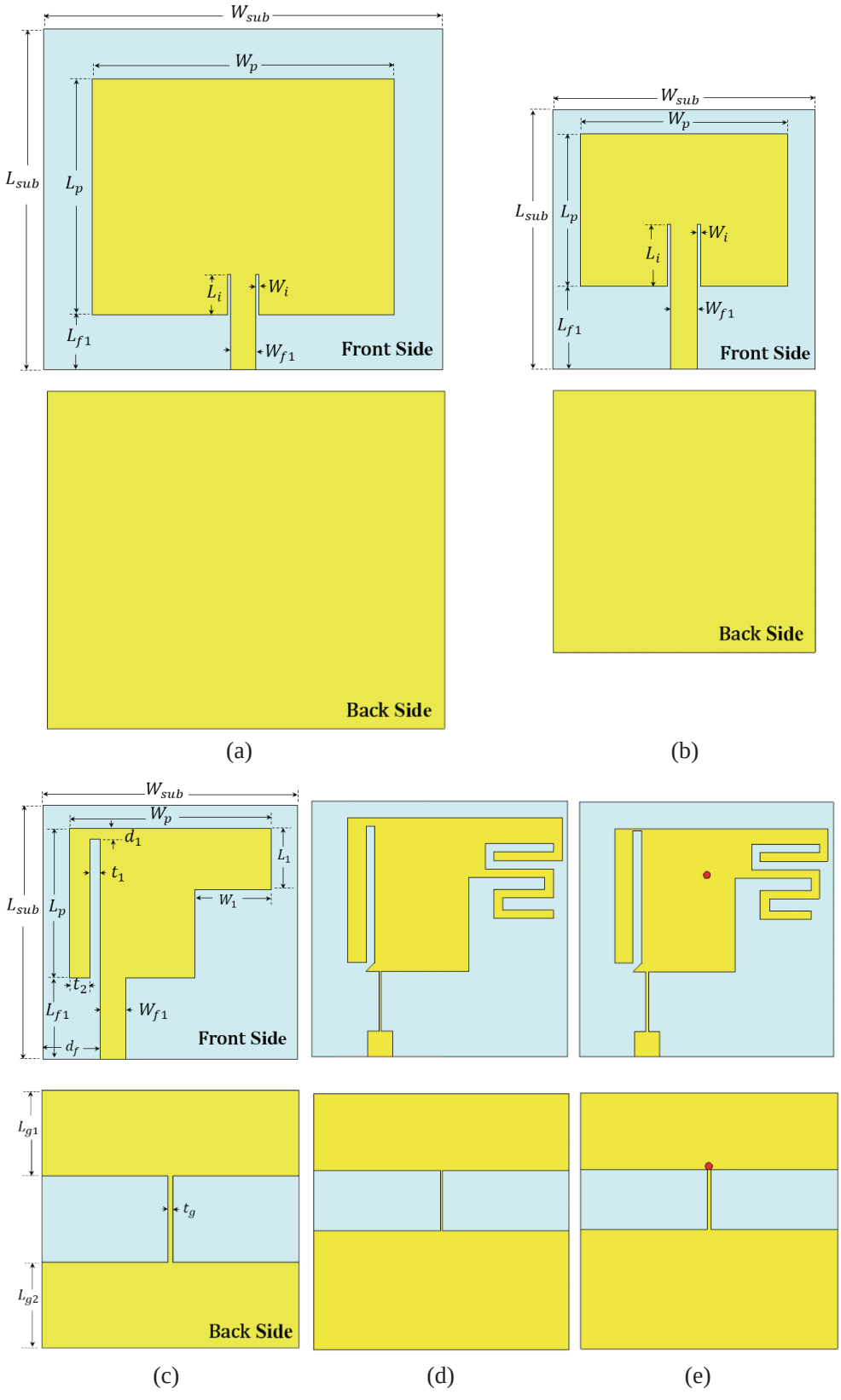


**Figure 1.** Antennas design steps. (a) Ant0. (b) Ant1. (c) Ant2. (d) Ant3. (e) Ant4.

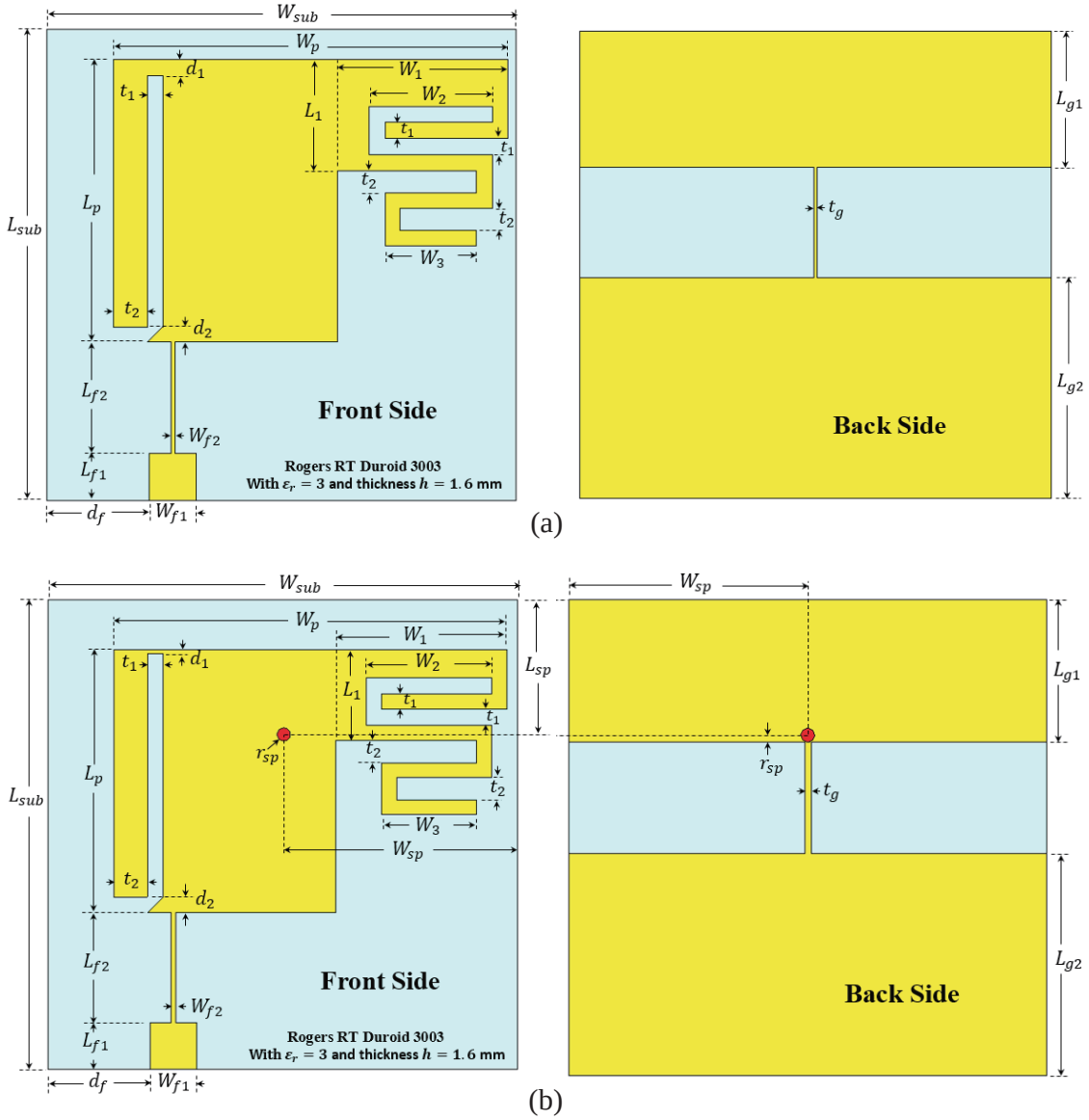


**Figure 2.** The proposed optimal CP antennas. (a) Without shorting pin. (b) With shorting pin.

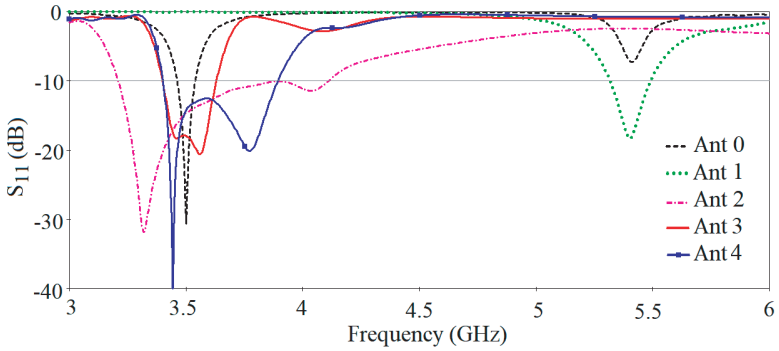


**Figure 3.** Simulated $S_{11}$ vs frequency (from 3 to 6 GHz) of the antenna designs in Fig. 1.

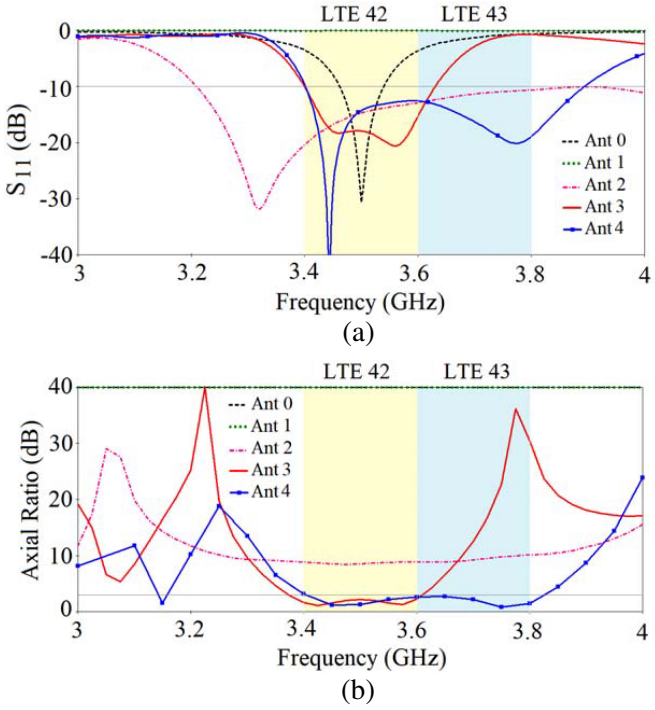


**Figure 4.** Simulated (a) $S_{11}$ and (b) axial ratio vs frequency (from 3 to 4 GHz) of the designed antennas in Fig. 1.

resonant frequency $f_r$, and the height of the substrate $h_{sub}$. The relationship among $W_p$, $L_p$, and other two parameters $\varepsilon_{reff}$, $\Delta L$ can be expressed [24] as

$$W_p = \frac{v_0}{2f_r}\sqrt{\frac{2}{\varepsilon_r+1}} \tag{1a}$$

$$L_p = \frac{v_0}{2f_r\sqrt{\varepsilon_{eff}}} - 2\Delta L \tag{1b}$$

$$\Delta L = 0.412h_{sub}\frac{(\varepsilon_{eff}+0.3)\left(\frac{W_p}{h_{sub}}+0.262\right)}{(\varepsilon_{eff}-0.258)\left(\frac{W_p}{h_{sub}}+0.8\right)} \tag{1c}$$

$$\varepsilon_{reff} = \frac{\varepsilon_r+1}{2}+\frac{\varepsilon_r-1}{2}\left(\frac{1}{\sqrt{1+12h_{sub}/W_p}}\right) \tag{1d}$$

where $v_0$, $\varepsilon_{reff}$, and $\Delta L$ denote the speed of light in the free space, effective dielectric constant, and the extension of the length, respectively.

Using (1), one can design a conventional RMA for operating at a resonant frequency $f_r = 3.5$ GHz (a center frequency of the LTE 42 band, 3.4–3.6 GHz) by using a substrate (Roger 3003) with $\varepsilon_r = 3$ and $h_{sub} = 1.6$ mm. So, the width $W_p = 30.30$ mm and length $L_p = 24.13$ mm are found. Then, a CST MWS is used as a simulation tool for this antenna to resonate at 3.5 GHz by using the patch dimensions $W_p \times L_p$ as 30.30 mm × 23.5 mm with specified substrate information and overall dimensions $W_{sub} \times L_{sub}$ of 40 mm × 34 mm. As shown in Fig. 3 and Fig. 4(a), Ant0 operates under its $TM_{010}$ mode with $f_{r1} = 3.5$ GHz. Also, it appears that the minimum $|s_{11}|$ occurs at $f_{r2} = 5.41$ GHz, which represents the second higher $f_r$ under a $TM_{002}$ mode, exhibiting a −10-dB impedance bandwidth (IBW) from 3.46 to 3.54 GHz or 2.28%. The value of $f_{r2}$ can be given by

$$f_{r2} = \frac{v_0}{\sqrt{\varepsilon_r}W_p} \tag{2}$$

**Table 1.** The optimal dimension parameters of the five designed antennas.

| Parameters | Values (mm) | | | | |
|---|---|---|---|---|---|
| | Ant0 | Ant1 | Ant2 | Ant3 | Ant4 |
| $W_{sub}$ | 40 | 25 | 25 | 25 | 25 |
| $L_{sub}$ | 34 | 25 | 25 | 25 | 25 |
| $h_{sub}$ | 1.6 | 1.6 | 1.6 | 1.6 | 1.6 |
| $W_p$ | 30.3 | 19.8 | 19.8 | 21.15 | 21.15 |
| $L_p$ | 23.5 | 14.7 | 14.7 | 15.15 | 14.15 |
| $L_{f1}$ | 5.5 | 8.0 | 8.0 | 2.5 | 2.5 |
| $W_{f1}$ | 2.5 | 2.5 | 2.5 | 2.5 | 2.5 |
| $L_i$ | 4.0 | 6.0 | - | - | - |
| $W_i$ | 0.3 | 0.3 | - | - | - |
| $d_f$ | - | - | 5.85 | 5.5 | 5.7 |
| $L_1$ | - | - | 6.0 | 5.9 | 4.9 |
| $W_1$ | - | - | 7.5 | 9.2 | 9.2 |
| $d_1$ | - | - | 1.0 | 0.84 | 0.2 |
| $t_g$ | - | - | 0.5 | 0.2 | 0.34 |
| $L_{g1}$ | - | - | 8.33 | 7.6 | 7.6 |
| $L_{g2}$ | - | - | 8.33 | 11.8 | 11.8 |
| $W_2$ | - | - | - | 6.7 | 6.7 |
| $W_3$ | - | - | - | 4.9 | 4.9 |
| $L_{f2}$ | - | - | - | 5.9 | 5.9 |
| $W_{f2}$ | - | - | - | 0.2 | 0.5 |
| $d_2$ | - | - | - | 0.84 | 0.84 |
| $t_1$ | - | - | - | 0.85 | 0.85 |
| $t_2$ | - | - | - | 1.45 | 1.45 |
| $r_{sp}$ | - | - | - | - | 0.7 |
| $L_{sp}$ | - | - | - | - | 7.25 |
| $W_{sp}$ | - | - | - | - | 12.5 |

which is calculated as 5.71 GHz after substituting $W_p = 30.3$ mm, $\varepsilon_r = 3$ and $v_0 = 3 \times 10^8$ m/s. As Fig. 4(b) shows, which represents the simulated axial ratio, Ant0 does not possess any feature of CP operation.

**Step 2:** In this step, Ant1 (see Fig. 1(b)) is produced as a result of designing RMA to operate under a $TM_{010}$ dominant mode of 5.4 GHz, i.e., Ant1 is forced to resonate at $f_{r2}$ of Ant0. The substitution of the specified information ($f_r = 5.4$ GHz, $\varepsilon_r = 3$ and $h_{sub} = 1.6$ mm) in Eq. (1) is considered responsible for yielding $W_p = 19.64$ mm and $L_p = 15.32$ mm. After utilizing a CST for simulating the designed antenna with aforementioned specification and total substrate dimensions $W_{sub} \times L_{sub}$ of 25 mm × 25 mm, one can note from Fig. 3 that Ant1 resonates at 5.4 GHz by using $W_p \times L_p$ of 19.8 mm × 14.7 mm. This antenna has 54% reduction in size compared to Ant0, and it is considered the reference antenna with all the remaining three antennas (Ant2, Ant3, and Ant4) designed on the $25 \times 25$ mm$^2$ sheet of Roger 3003 with a thickness of 1.6 mm, dielectric constant of 3, and loss tangent of 0.001. Also, as depicted in Fig. 4(b), no feature for CP is achieved from this antenna.

**Step 3:** This third step produces Ant2, as shown in Fig. 1(c), after developing Ant1 for reducing the axial ratio closer towards CP and enlarging the current path to operate at the LTE 42 band (3.4–3.6 GHz). This is done by etching a notch of width $t_1$ into a distance $d_1$ at the left side of the patch and

making the right side of the patch as a stair-shaped geometry (within it a one meander-line structure will be used for Ant3 and Ant4) with dimension $W_1 \times L_1$. Also, offset feedline, at distances $d_f$ from the left side of the substrate and $t_1 + t_2$ from the left side of the patch, is used instead of the previous feedline. On the back side of the substrate, the ground plane is made as a rotated H-shaped capital letter with lengths of its two main strips $L_{g1} = L_{g2} = L_{sub}/3$ and thickness of the secondary arm connecting the main arms denoted as $t_g$. As noted in Fig. 3 and Fig. 4(a), a wide $-10$-dB IBW ranging from 3.21 to 4.11 GHz is provided from Ant2 with the minimum value $s_{11}$ of $-31.83$ dB taking place at 3.32 GHz. Fig. 4(b) depicts that there is an ability by this antenna to be optimized for having a CP characteristic in its operation and providing the desired $-3$-dB axial ratio bandwidth (ARBW) covering the LTE 42 (3.4–3.6 GHz) alone or both LTE 42 and LTE 43 (3.6–3.8 GHz) bands. This is satisfied by fine tuning some affecting geometric antenna parameters and/or adding a shorting pin at a specific location for enhancing CBW, i.e., both IBW and ARBW, via using PSO in conjunction with CST software to get the optimized designed antennas, Ant3 and Ant4, which will be described in the following design step 4.

**Step 4:** This final design step presents the two optimized CP antennas, Ant3 and Ant4, with and without shorting pin, as shown in Figs. 1(d) and (e), respectively, and the detailed structures of them are depicted in Fig. 2. The simulated reflection coefficient and axial ratio results of these two optimized CP antennas are shown in Figs. 3, 4(a) and Fig. 4(b), respectively. The next section introduces the detailed description of applying the optimization methodology for designing the proposed antennas to satisfy the specified performance. This performance includes the enhancement of both the voltage standing wave ratio bandwidth (VRBW) and 3-dB ARBW, i.e., the CBW, in addition to realized gain (RG) greater than a threshold value of 2 dB.

As shown in Figs. 2(a) and (b) for both antennas (Ant3 and ant4), an offset 50 Ω microstrip line is placed at a distance $d_f$ from the left side of the patch of size $W_p \times L_p$, and this feedline has two different sizes of $W_{f1} \times L_{f1}$ and $W_{f2} \times L_{f2}$, which are used for improving the impedance bandwidth. Two meandered-line shaped structures, as a one-turn slot of thickness $t_1$ and arm width $W_2$ and the other as two-turn strips of thickness $t_1$, spacing between turns $t_2$ and arm width $W_3$, and placed on the upper right side of the patch. At a distance of $t_2$ from the patch's lower left side, a slit of width $t_1$ is removed until a distance $d_1$. Also, a triangular strip of lengths $d_2$ and $t_1$ is placed on the lower left side of the patch. This antenna of an overall size $W_{sub} \times L_{sub}$ with a value of 25 mm × 25 mm is printed on the top side of a semi-flexible Roger 3003 substrate, having a dielectric constant of 3, loss tangent of $\tan\delta = 0.001$, and thickness of 1.6 mm. To improve both IBW and ARBW, the back of the substrate is made as a 90° rotated H-shaped capital letter geometry with the main unsymmetrical arms' dimensions, denoted by $L_{g1}$ and $L_{g2}$, and the width of the arm section connected the main arms is represented by $t_g$.

More flexibility for CBW enhancement during optimization process is obtained by adding a shoring pin to Ant4 of radius $r_{sp}$, and its location is specified by horizontal and vertical distances $W_{sp}$ and $L_{sp}$, respectively, see Fig. 2(b). As Figs. 4(a) and (b) show, Ant3 (Ant4) covers LTE 42 (LTE 42/43) band, i.e., covering frequencies from 3.4 to 3.6 GHz (3.4 to 3.8 GHz).

## 3. PROBLEM FORMULATION OF THE OPTIMAL CP ANTENNA

In this section, a new general optimization procedure for designing an optimally CP antenna is presented. Firstly, the problem formulation is defined as an optimization problem with the broadest CBW (VRBW + ARBW) and highest RG in the forward direction. Secondly, this optimization methodology, based on conjunction of particle swarm optimization (PSO) implemented in MATLAB and CST software, is applied as an illustrative example for finding the two optimized CP antennas, with and without shorting pin, described in the previous section.

### 3.1. Optimization Problem Formulation

The optimal antenna design task is defined as ($\mathbf{x}$ being a vector containing geometry parameters). Then, the proposed fitness function of the optimal CP antenna is formulated as:

$$\mathbf{x}^* = \arg\max_x F(\mathbf{x}, f) \tag{3a}$$

where

$$F(\mathbf{x}, f) = F_{abs} F_{sign} \tag{3b}$$

In (3), the fitness function $F(\mathbf{x}, f)$ to be maximized is formulated by multiplying two functions $F_{abs}$ and $F_{sign}$, which are introduced for evaluating the absolute and sign values of $F(\mathbf{x}, f)$, respectively, and can be expressed as

$$F_{abs} = 10^{12} \left( \prod_{i=1}^{3} \left|\Delta f_L^i\right| \left|\Delta f_H^i\right| \right) \left( \prod_{i=1}^{3} \left|\Delta s_L^i\right| \left|\Delta s_H^i\right| \right) \tag{4a}$$

$$F_{sign} = 2 \left[ \left( \sum_{i=1}^{3} u\left(\Delta f_L^i\right) + u\left(\Delta f_H^i\right) \right) + \left( \sum_{i=1}^{3} u\left(\Delta s_L^i\right) + u\left(\Delta s_H^i\right) \right) \right] - 1 \tag{4b}$$

In (4), $\prod(\cdot)$ and $\sum(\cdot)$ represent the multiplication and summation factors; $|\cdot|$ denotes an absolute operator; $u(\cdot)$ is a unit step function; and the three pluses denoted by "+" within the brackets are equivalent to the logical AND operation. The other symbols or variables in (4) are defined as follows

$$\Delta f_L^i = f_L^d - f_L^i \tag{5a}$$

$$\Delta f_H^i = -f_H^d + f_H^i \tag{5b}$$

$$\Delta s_L^i = c_i - s_L^i \tag{5c}$$

$$\Delta s_H^i = c_i - s_H^i \tag{5d}$$

where

$$f_L^i = f \left| \begin{array}{l} S_i(\mathbf{x}, f) = c_i \\ \frac{\partial S_i(\mathbf{x}, f)}{\partial f} < 0 \end{array} \right. \tag{6a}$$

$$f_H^i = f \left| \begin{array}{l} S_i(\mathbf{x}, f) = c_i \\ \frac{\partial S_i(\mathbf{x}, f)}{\partial f} > 0 \end{array} \right. \tag{6b}$$

and

$$s_L^i = S_i(\mathbf{x}, f)|_{f=f_L^d} \tag{7a}$$

$$S_H^i = S_i(\mathbf{x}, f)|_{f=f_H^d} \tag{7b}$$

In (5a) and (5b), $\Delta f_L^i (\Delta f_H^i)$ represents the $i$th lower (higher) difference frequency between the desired lower (higher) frequency $f_L^d (f_H^d)$ and the $i$th lower (higher) frequency $f_L^i$ $(f_H^i)$. In (5c) and (5d), $\Delta s_L^i$ $(\Delta s_H^i)$ denotes the difference between the $i$th antenna performance function $S_i(\mathbf{x},f)$ and its $i$th constraints $c_i$ at $f_L^d (f_H^d)$. The two frequencies $f_L^i$ and $f_H^i$, expressed in (6a) and (6b), are defined as frequencies over which the function $S_i(\mathbf{x},f) = c_i$ and its slope $\partial S_i(\mathbf{x}f)/\partial f$ is less or greater than zero, respectively. The two symbols $s_L^i$ and $s_H^i$, represented by (7a) and (7b), are defined as the values of $S_i(\mathbf{x},f)$ at the operating frequency $f = f_L^d$ and $f = f_H^d$, respectively.

As noticed in (4a), $F_{abs}$ has an absolute numeric value ($\geq 0$), and it is written by multiplying two multiplicative functions, in which each one is calculated for $i$= 1 to 3, corresponding to the three antenna performance functions defined by $S_i(\mathbf{x},f)$, and all must be maximized at once. In (4b), $F_{sign}$ has either a value "1" or "−1" depending on the state of its two summations (binary addition), with each one calculated for the three cases of $S_i(\mathbf{x},f)$ and $u(\cdot)$ function. Thus, $F_{sign} = 1$ if all four differences of the three antenna performances are greater than zero (or positive values); otherwise, $F_{sign} = -1$ whenever one of the four above-mentioned difference parameters in the three cases is less than zero (or negative value). In this work, $S_i(\mathbf{x},f)$ and $c_i$ can be expressed as

$$S_i(\mathbf{x},f) = \begin{cases} VR(\mathbf{x},f) & \text{if} \quad i\text{= 1, } VRBW \\ AR(\mathbf{x},f) & \text{if} \quad i\text{= 2, } ARBW \\ -G(\mathbf{x},f) & \text{if} \quad i\text{= 3, } RG \end{cases} \tag{8a}$$

$$c_i = \begin{cases} 2.0 & \text{if} \quad i\text{= 1, } VRBW \\ 2.0\,(3\,\text{dB}) & \text{if} \quad i\text{= 2, } ARBW \\ 1.6\,(2\,\text{dB}) & \text{if} \quad i\text{= 3, } RG \end{cases} \tag{8b}$$

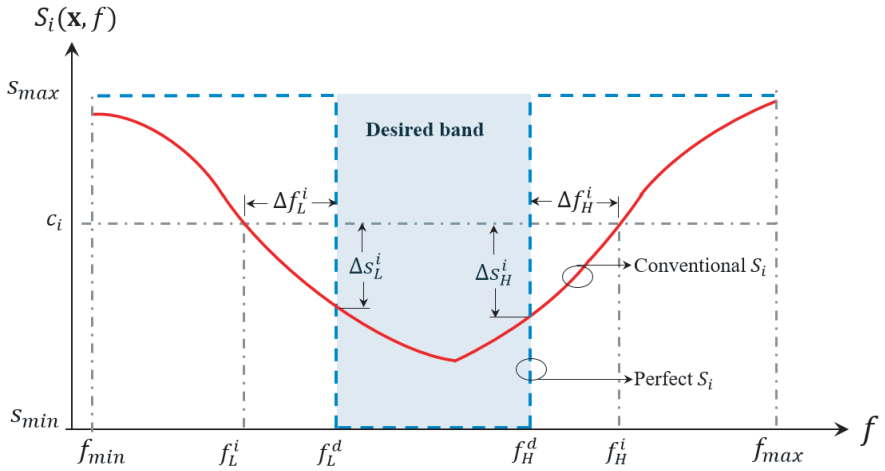


**Figure 5.** Demonstration of conventional and perfect $S_i(\mathbf{x},f)$ performance function for the optimal CP antenna.

The conventional and perfect $S_i(\mathbf{x},f)$ performance of the optimal antenna for being operating at a desired frequency band ($f_L^d \leq f \leq f_H^d$) is depicted in Fig. 5. As noticed from this figure, an efficient design optimality is obtained for $F(\mathbf{x},f) \geq 0$ with a maximum value ($F_{\max}$) when all the following four criteria, for $i = 1, 2, 3$ defined in (5a)–(5d), are satisfied:

$$\Delta f_L^i > 0 \quad \text{or} \quad f_L^i < f_L^d \tag{9a}$$

$$\Delta f_H^i > 0 \quad \text{or} \quad f_H^i > f_H^d \tag{9b}$$

$$\Delta s_L^i > 0 \quad \text{or} \quad S_i(\mathbf{x}, f)|_{f=f_L^d} < c_i \tag{9c}$$

$$\Delta s_H^i > 0 \quad \text{or} \quad S_i(\mathbf{x}, f)|_{f=f_H^d} < c_i \tag{9d}$$

In this work for $S_i(\mathbf{x},f)$ defined in (8a), $VR(\mathbf{x},f)$ is considered the main performance function while $AR(\mathbf{x}, f)$ and $G(\mathbf{x},f)$ represent the secondary performance functions that must perform the following three desired performances for the optimal CP antenna design:

a) The best antenna bandwidth is defined by: $VR(\mathbf{x}, f) = \max\{f_L^d \leq f \leq f_H^d : VR(\mathbf{x},f)\}$ and $f$ is a frequency within a range of interest ($f_{\min} \leq f \leq f_{\max}$), and $f_L^d$ and $f_H^d$ are the desired lower and higher frequencies of the desired band, respectively, with the constraint $VR(\mathbf{x},f) < 2.0$.

b) Axial ratio improvement is calculated by: $AR(\mathbf{x}, f) = \max\{f_L^d \leq f \leq f_H^d : AR(\mathbf{x},f)\}$ with the constraint $AR(\mathbf{x},f) < 2(3\,\text{dB})$.

c) Gain maximization is achieved by using: $-G(\mathbf{x},f) = \max\{f_L^d \leq f \leq f_H^d : G(\mathbf{x},f)\}$ with the constraint $G(\mathbf{x},f) \geq 1.6(2\,\text{dB})$.

As a summary of what has been presented, this method is considered new and not used previously in the literature and can be applied to any designed antenna to be optimized for having the feature of circular polarization operation.

### 3.2. Design of Optimized CP Antennas

The aforementioned simulated $s_{11}$ and AR performance results presented in Sec. 2, as depicted in Figs. 2 and 4, for the two CP antennas (with and without shorting pin), i.e., Ant3 and Ant4, will be validated by the proposed optimization method. This includes improving both their ARBW and IBW while maintaining a moderate RG across the desired whole operating frequency band, LTE 42 (3.4–3.6 GHz), or LTE 42/43 (3.4–3.8 GHz) band, respectively. To operate at these two bands, the desired lower and higher frequencies $f_L^d$ and $f_H^d$ used for finding the optimal CP antennas are defined in Table 2. Firstly, Ant3 is optimized for finding its optimal dimensions, and after that the optimization methodology

**Table 2.** The desired frequencies $f_L^d$ and $f_H^d$ constitute the desired frequency bands used in the design optimization methodology for the proposed CP antennas, Ant3 and Ant4.

| Desired frequency | Ant3 | | Ant4 | |
|---|---|---|---|---|
| | $f_L^d$ | $f_H^d$ | $f_L^d$ | $f_H^d$ |
| Value (GHz) | 3.4 | 3.6 | 3.4 | 3.8 |

**Table 3.** Antenna geometric parameters that are unvaried during optimization.

| Parameter | $W_{sub}$ | $L_{sub}$ | $h_{sub}$ | $W_{f1}$ | $L_{f1}$ | $W_{sp}$ | $d_f$ |
|---|---|---|---|---|---|---|---|
| Value (mm) | 25 | 25 | 1.6 | 2.5 | 2.5 | 12.5 | 5.7 |

**Table 4.** Ranges that allowed to be varied during optimization of the geometric parameters and their optimized dimensions. Legend: NC: Not Changed, NA: Not Available.

| Parameter | Range (mm) | | Optimized dimension (mm) | |
|---|---|---|---|---|
| | Ant3 | Ant4 | Ant3 | Ant4 |
| $W_1$ | $7.2 \sim 9.2$ | NC | 9.2 | 9.2 |
| $W_2$ | $4.0 \sim 7.0$ | NC | 6.7 | 6.7 |
| $L_1$ | $4.0 \sim 8.0$ | $4.0 \sim 8.0$ | 5.9 | 4.9 |
| $t_1$ | $0.5 \sim 1.0$ | NC | 0.85 | 0.85 |
| $t_2$ | $1.0 \sim 2.0$ | NC | 1.45 | 1.45 |
| $d_1$ | $0.5 \sim 1.0$ | $0.5 \sim 1.0$ | 0.84 | 0.2 |
| $d_2$ | $0.5 \sim 1.0$ | NC | 0.84 | 0.84 |
| $L_{f2}$ | $5.0 \sim 7.0$ | NC | 5.9 | 5.9 |
| $W_{f2}$ | $0.2 \sim 2.5$ | $0.2 \sim 2.5$ | 0.2 | 0.5 |
| $L_{g1}$ | $6.25 \sim 8.33$ | NC | 7.6 | 7.6 |
| $L_{g2}$ | $8.33 \sim 12.5$ | NC | 11.8 | 11.8 |
| $t_g$ | $0.2 \sim 1.0$ | NC | 0.2 | 0.34 |
| $L_{sp}$ | NA | $5 \sim 15$ | 7.25 | NA |

is applied for Ant4. During the optimization of Ant3, seven parameters are unchanged while twelve geometric antenna parameters (i.e., $N_g = 12$) are allowed to be varied within their specified ranges, as listed in Tables 3 and 4, respectively.

Then, depending on the optimal simulated $s_{11}$ and AR performance results and parameters study of Ant3 in addition to reducing the time of the process, only four geometric parameters, i.e., $N_g = 4$ are allowed to be changed when finding an optimal CP antenna with shorting pin or Ant4. The range of other geometric parameters, denoted by a legend (NC: Not Changed) in Table 4, maintains the same optimized values obtained for Ant3. A PSO optimization algorithm implemented in MATLAB in conjunction with CST software is used for finding the optimal CP antennas by applying the fitness function $F(\mathbf{x}, f)$ defined in Sec. 2. In this work for Ant3 and Ant4, the number of particles $N_p$ is used as $5N_g$, i.e., $N_p = 60$ or 20 for $N_g = 12$ and 4, respectively. For the two antennas, the first generation of the optimization process is started by initializing PSO particles $N_p$ to be within the ranges of the geometric parameters allowed to be varied. During the optimization progress aiming to maximize $F(\mathbf{x}, f)$, the PSO particles are updated, and their values are exported to CST for changing the corresponding geometric antenna parameters. To have a good convergence rate with an acceptable time of processing, one of the

two criteria is used for stopping the optimization process, either $F(\mathbf{x},f) \geq 0$ with a maximum value of $F_{\max}$ is achieved or a maximum number of generations $N_{\max} = 100$ is reached.

Table 4 summarizes the optimized dimensions of both antennas (Ant3 and Ant4) after the optimization reached the specified stopping criterion limit of $N_{\max} = 100$. Fig. 6 shows the optimal CST simulated results, VSWR and axial ratio (AR) besides realized gain (RG) in linear scale. It is observed that the CBW is achieved for both antennas (Ant3 and Ant4) across their desired bands, LTE 42 and LTE 42/43. However, the RG is somewhat below the constrained value of $c_3 = 1.6$ (2 dB) at certain higher frequencies in LTE 42 and/or LTE 42/43 for Ant3 and Ant4, respectively. The defined parameters that entered formula of the fitness function, for the three performance results $S_i(\mathbf{x},f)$ of Fig. 6, are summarized in Table 5. These values (each value of the frequency in this table is used as it is, i.e., merely a normalized frequency in Hz, e.g., 3.397 not 3.397 GHz) are used in the fitness function $F(\mathbf{x},f)$ for the three values of $S_i(\mathbf{x},f)$. One can find that $F_{\max} = -0.507$ and $F_{\max} = -0.025$ for Ant3 and Ant4 or CP antenna with and without shorting pin, respectively, which both are nearly close to zero, especially Ant4. These results demonstrate that the presented optimization methodology can be eligibly used for finding optimal antennas with the broadest CBW and feature of CP operation and an acceptable realized gain across the desired frequency band.

**Table 5.** The values of $i$th lower and higher frequencies $f_L^i$ and $f_H^i$ besides the $i$th lower and higher values $s_L^i$ and $s_H^i$, respectively, of the three performance functions $S_i(\mathbf{x},f)$ for $i = 1, 2, 3$. The unit of frequency is (GHz).

| $i$ | $S_i(\mathbf{x},f)$ | CP antenna without shorting pin | | | | CP antenna with shorting pin | | | |
|---|---|---|---|---|---|---|---|---|---|
| | | $f_L^i$ | $f_H^i$ | $s_L^i$ | $s_H^i$ | $f_L^i$ | $f_H^i$ | $s_L^i$ | $s_H^i$ |
| 1 | $VR(\mathbf{x},f)$ | 3.397 | 3.634 | 1.917 | 1.415 | 3.397 | 3.900 | 1.976 | 1.255 |
| 2 | $AR(\mathbf{x},f)$ | 3.335 | 3.648 | 1.205 | 1.309 | 3.356 | 3.869 | 1.453 | 1.190 |
| 3 | $-G(\mathbf{x},f)$ | 3.423 | 3.533 | 1.398 | 1.408 | 3.405 | 3.500 | 1.534 | 1.494 |

## 4. PARAMETRIC ANALYSIS OF THE OPTIMAL ANTENNAS

This section presents a detailed parametric analysis of functional geometric parameters ($d_1$, $L_1$ and $W_{f2}$) of the two designed CP antennas besides shorting pin parameters ($W_{sp}$ and $L_{sp}$), on return loss and axial ratio characteristics. Then, to validate that the proposed antennas has the feature of CP operation, and a simulated current distribution over frequency bands of interest is presented. To accurately determine the influence of these five parameters on antenna performance, each parameter is allowed to be varied alone at a time, and the others maintain their optimized values as listed in Table 4.

Figure 7(a) shows the influence of varying $d_1$ on IBW and ARBW, i.e., −10-dB $S_{11}$ impedance and 3-dB axial ratio bandwidths, respectively. As the value is varied from 0.3 mm to 1.0 mm (0.5 mm to 1.0 mm), the lower frequency band of the reflection coefficient graph is tuned much lower for $d_1 = 1.0$ mm (0.5 mm) for CP antenna without (with) shorting pin. On the other hand, it is noticed that the higher frequency band is nearly unaltered, and both antennas have a balance kept in tuning the upper-frequency ranges in the desired frequency bands. As Fig. 7(a) shows, a broader ARBW is obtained satisfying the desired LTE 42 (LTE 42/43) for CP antenna without (with) pin as $d_1 = 0.5$ mm ($d_1 = 1.0$ mm).

Figure 7(b) depicts the effect of varying the length $L_1$ on $S_{11}$ and axial ratio plots of the antenna without (with) shorting pin as the value increases from 4.0, 4.9 to 7.5 mm (4.0, 5.9 to 7.5 mm). It is noticed that, for antenna without pin, a significant effect occurs in the lower band of the reflection coefficient plot. It starts to deteriorate as $L_1$ becomes 4 mm, and the higher-frequency band is nearly not altered, whereas dual-frequency bands are created in $S_{11}$ plot of antenna with shorting pin when $L_1$ has a value of 4 mm. The axial ratio curve of antenna without pin becomes greater than 3 dB for lower value of $L_1 = 4.0$ mm making the desired band disappear, and two bands arise as $L_1 = 7.5$ mm. On the other hand, dual-frequency band in AR plot of antenna with pin is noticed as the value of $L_1$ is 4.0 and 7.5 mm with approximately unchanging in the upper-frequency band.

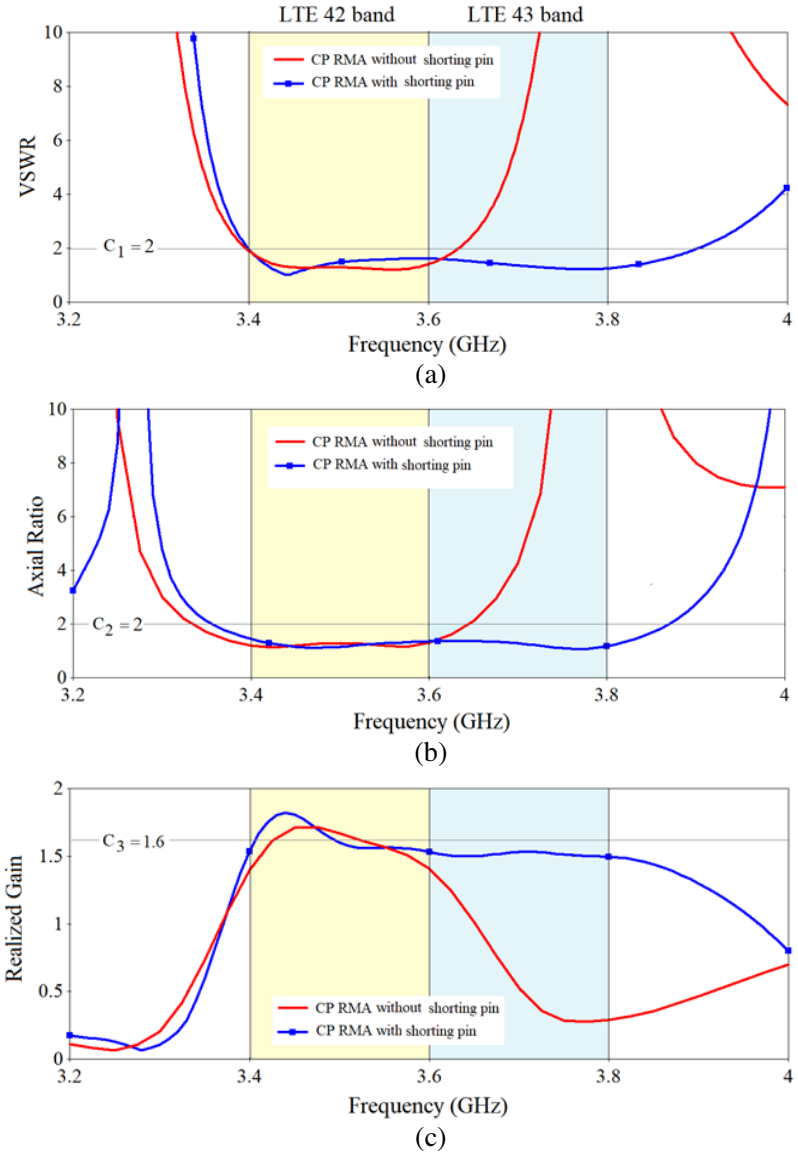


**Figure 6.** Simulated results of the optimal deigned CP antennas. (a) VSWR. (b) Axial ratio. (c) Realized gain.

It can be observed from Fig. 7(c) that when a value of the feed width $W_{f2}$ is 0.5 mm, the $S_{11}$ plots of both antennas (with and without pin) begin to shift up making IBW have a lower value resulting from upshifting and downshifting of the lower and upper frequency bands, respectively. As $W_{f2}$ ascends to a maximum value of 2.5 mm, the whole $S_{11}$ curves for both the antennas over the operating frequency range (3.2 to 4.0 GHz) become above the −10-dB line, resulting in the disappearance of IBWs. Also, as the value of $W_{f2}$ increases, the ARBWs for both the antennas start to decrease, and dual-band frequency is observed. Hence, a nominal value of 0.5 mm (0.25 mm) is an optimal value chosen for CP antenna without (with) shorting pin to cover the desired frequency bands concerning both IBW and ARBW.

Figures 7(d) and (e) depict the impact of varying the location of a shorting pin of the CP antenna, specified by the two parameters ($L_{sp}$ and $W_{sp}$), on the $S_{11}$ and AR characteristics. It can be observed from Fig. 7(d) that increasing $W_{sp}$ from 5.0 mm to 10.0 mm with a step size of 2.5 mm, the lower impedance frequency is slightly upshifting whereas the higher frequency is largely decreased to less

than 3.6 GHz for $W_{sp}$ = 10.0 mm, and it is nearly unchanged with a value greater than 3.8 GHz for $W_{sp}$ = 5.0 mm. As Fig. 7(d) shows, as the value of $W_{sp}$ is 10 mm, ARBW is decreased within a range of frequencies, less than 3.5 GHz and greater than 3.3 GHz, and narrow dual-frequency bands are generated, one around 3.4 GHz and the other about a frequency of 3.8 GHz. In Fig. 7(e), as $L_{sp}$ is varied from 5.0 mm to 10 mm, the lower frequency of $S_{11}$ plot is almost unaffected for $L_{sp}$ = 5.0 mm; the higher frequency is decreased; and the whole $S_{11}$ plot becomes less than −10 dB for $L_{sp}$ = 10 mm. On the other hand, as noticed in Fig. 7(e), the lower frequency of the AR plots is slightly altered as the values of $W_{sp}$ are varied within the range (5.0 and 10 mm), but the upper frequency decreases from a desired upper frequency of 3.8 GHz when $W_{sp}$ has a value of 10 mm. Above all, loaded shorting pin, meander line shape, feed width, and the loaded slot strip are key parameters for providing the required impedance and axial ratio bandwidths that are necessary for CP antenna.

To confirm that the two antennas have the feature of CP operation over the desired frequency bands, Figs. 8(a) and (b) depict the surface current distribution at 3.5 and 3.6 GHz (center frequencies) for antenna without and with shorting pin, respectively. As noticed in Figs. 8(a) and (b), the surface currents flow in a clockwise direction, and a Left Hand Circular Polarizd (LHCP) radiation is produced as both two antennas having maximum radiation for 3.5 GHz and 3.6 GHz in the broadside direction outward (+$z$-axis), respectively. The proposed antennas can easily produce a Right Hand Circularly Polarized (RHCP) radiation by mirroring the meander line-shaped structure in the patch plane.

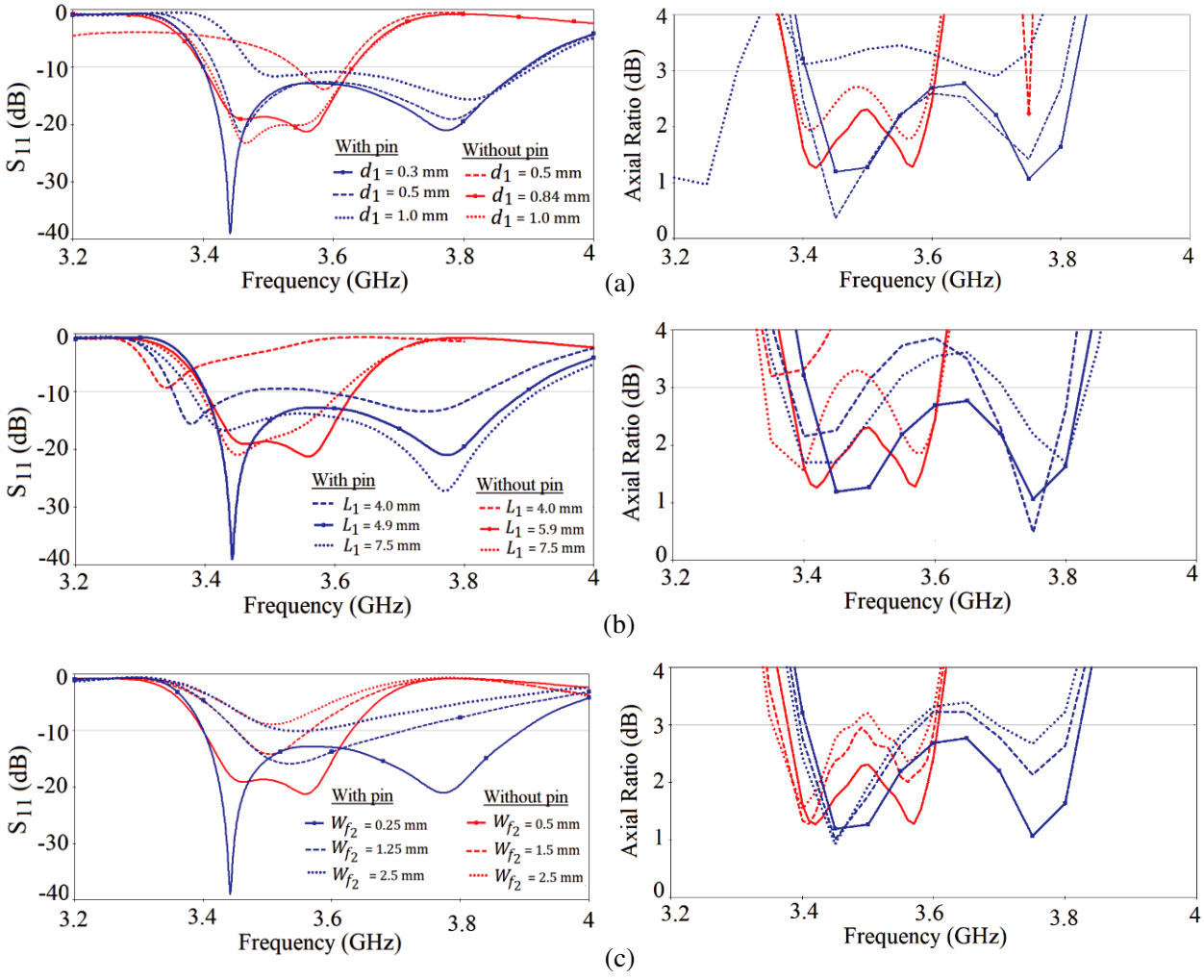

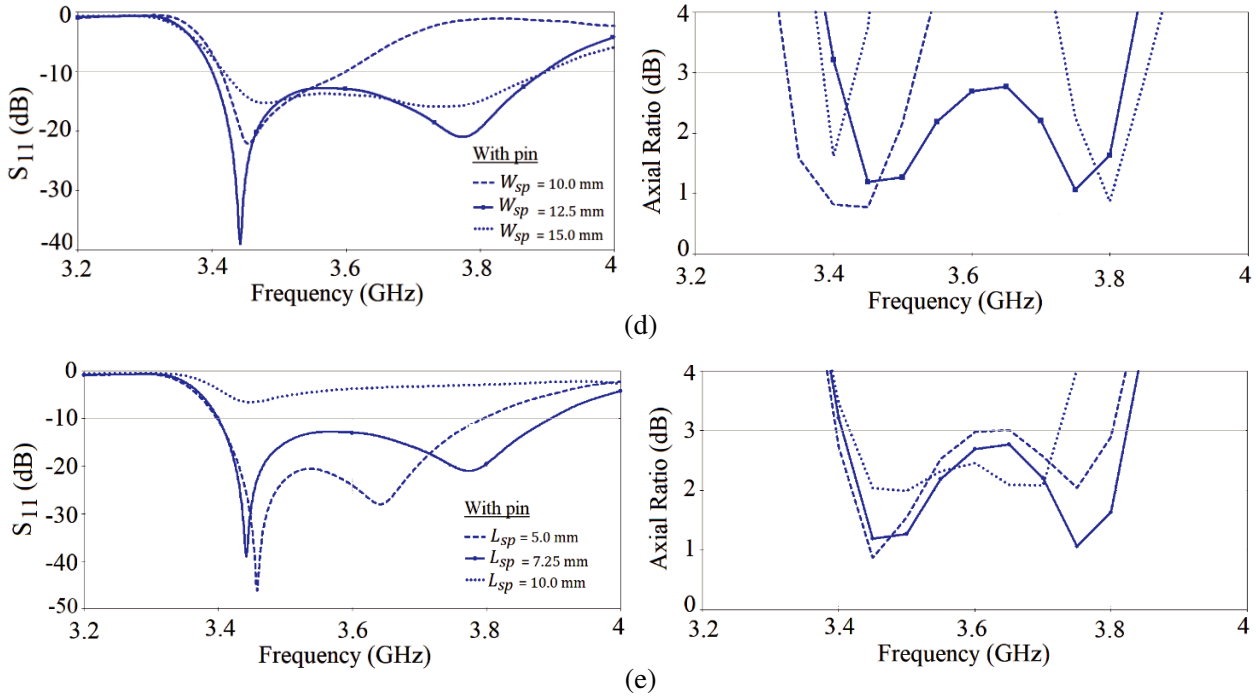


**Figure 7.** Influence of (a) $d_1$, (b) $L_1$, (c) $W_{f2}$, (d) $W_{sp}$ and (e) $L_{sp}$ on antenna performance: Reflection coefficient (left); Axial ratio (right).

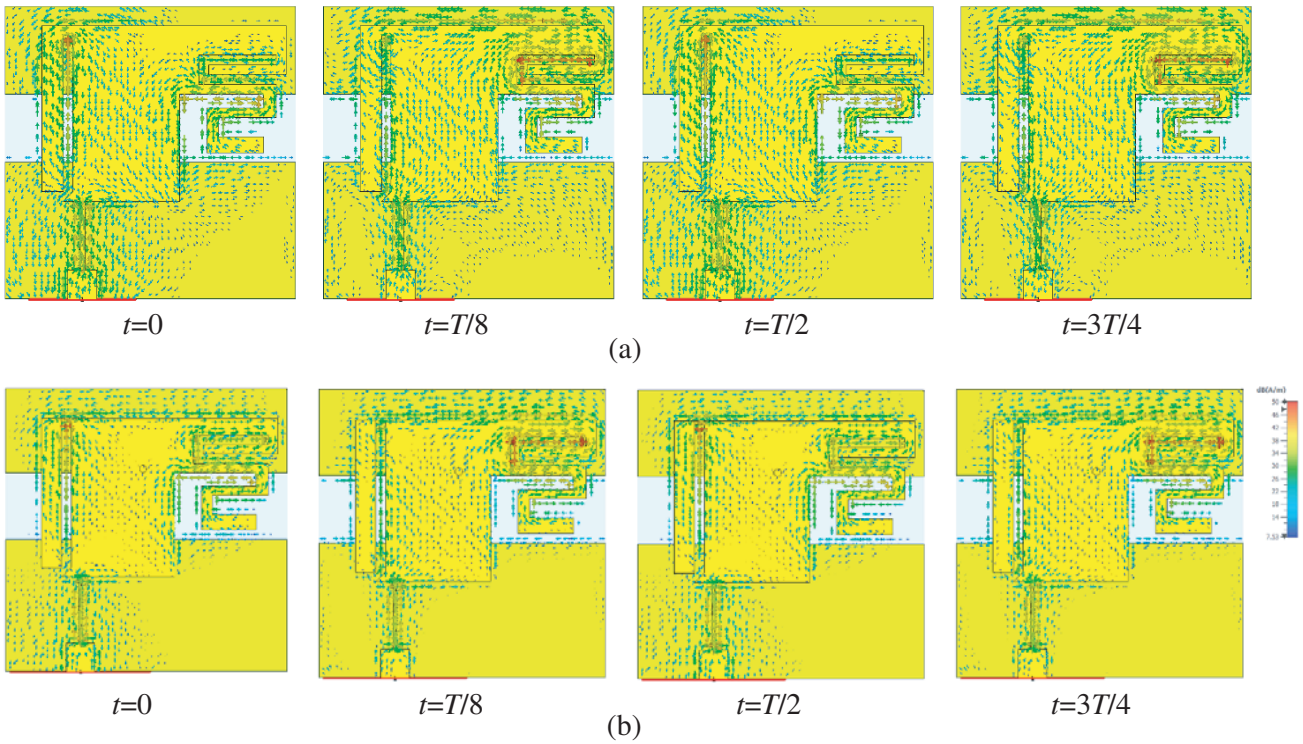


**Figure 8.** Simulated Surface current distributions at 3.5 GHz for CP antenna, (a) without and (b) with shorting pin.

## 5. EXPERIMENTAL AND SIMULATED RESULTS AND DISCUSSION

In the previous section, the CP antennas with and without shorting pin were successfully designed to cover the desired frequency bands (LTE 42 and LTE 42/43) using the proposed optimization methodology, and a CST MWS was adopted as a simulator tool for analyzing and simulating those antennas. Photographs of the fabricated antennas designs without and with shorting pin and the measurement setup in an anechoic chamber are shown in Fig. 9. The simulated and measured $S_{11}$ and axial ratio plots of the two antennas are shown in Figs. 10(a) and (b), whereas the gain and efficiency characteristics are depicted in Figs. 11(a) and (b), respectively.

Table 6 summarizes the aforementioned results of Fig. 10, which include the lower and higher frequencies $f_L$ and $f_H$, respectively in addition to resonance frequencies $f_{r1}$ and $f_{r2}$ of the IBW and ARBW. The simulated and measured antenna gains and efficiencies of Figs. 11(a) and (b) at the above-mentioned four frequencies are listed in Table 7. As noticed from Fig. 10 and Table 6, the simulated and measured $f_L$, $f_H$, $f_{r1}$, and $f_{r2}$ are in good agreement, validating the design concept. Also, the IBWs for the antennas without (with) shorting pin are 240 and 220 MHz (510 and 460 MHz) whereas the

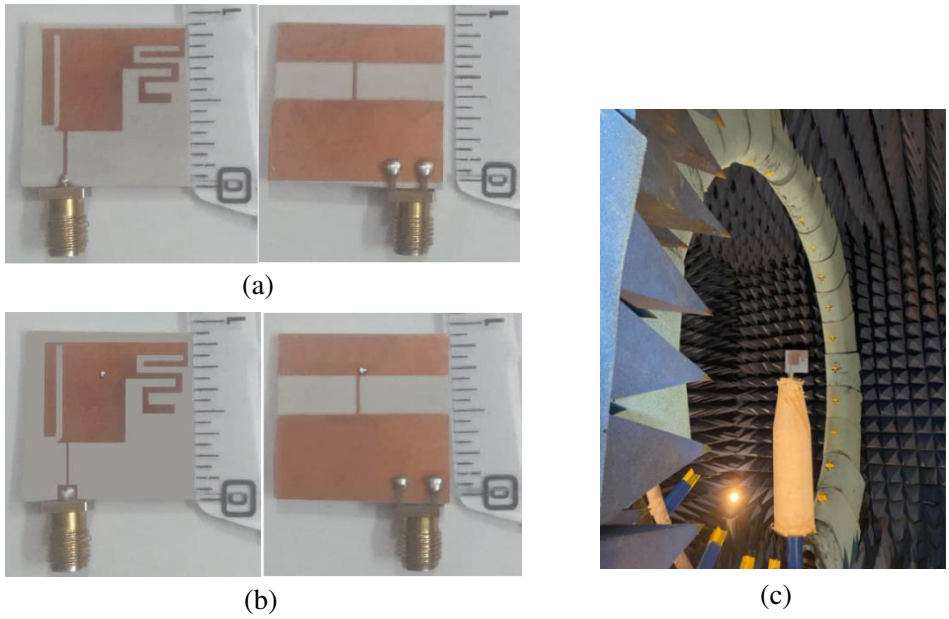


**Figure 9.** Photograph of the fabricated CP antennas designs (a) without and (b) with shorting pin under the same physical size. (c) Measurement setup in anechoic chamber.

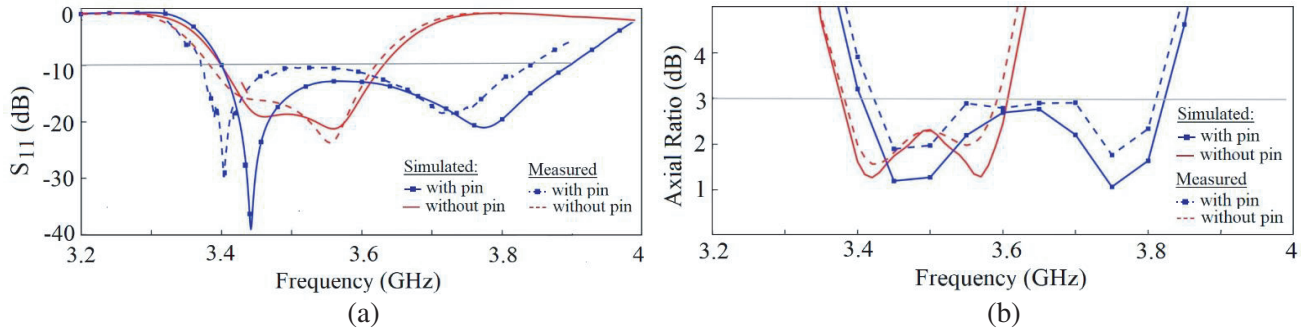


**Figure 10.** Simulated and measured (a) $S_{11}$ and (b) Axial ratio of the optimal deigned CP antennas without and with shorting pin.

**Table 6.** Comparison of the measured and simulated IBW and ARBW results of the prposed antennas.

| Antenna Performance | | CP antenna without shorting pin | | | | CP antenna with shorting pin | | | |
|---|---|---|---|---|---|---|---|---|---|
| | | $f_L$ | $f_H$ | $f_{r1}$ | $f_{r2}$ | $f_L$ | $f_H$ | $f_{r1}$ | $f_{r2}$ |
| IBW | simulated | 3.39 | 3.63 | 3.45 | 3.56 | 3.39 | 3.90 | 3.44 | 3.77 |
| | measured | 3.38 | 3.6 | 3.44 | 3.55 | 3.37 | 3.83 | 3.4 | 3.72 |
| ARBW | simulated | 3.33 | 3.65 | 3.42 | 3.56 | 3.36 | 3.87 | 3.44 | 3.75 |
| | measured | 3.4 | 3.6 | 3.42 | 3.55 | 3.42 | 3.81 | 3.45 | 3.75 |

**Table 7.** Comparison of the measured and simulated gain and efficiency of the proposed antennas.

| Antenna Performance | | CP antenna without shorting pin | | | | CP antenna with shorting pin | | | |
|---|---|---|---|---|---|---|---|---|---|
| | | @$f_L$ | @$f_H$ | @$f_{r1}$ | @$f_{r2}$ | @$f_L$ | @$f_H$ | @$f_{r1}$ | @$f_{r2}$ |
| Gain (dB) | simulated | 1.53 | 1.44 | 2.16 | 2.0 | 2.0 | 1.2 | 2.39 | 1.79 |
| | measured | 1.26 | 1.2 | 1.93 | 1.92 | 2.5 | 2.0 | 2.74 | 2.34 |
| Efficency(%) | simulated | 86 | 91 | 96.2 | 95.9 | 81 | 75 | 92.5 | 86.5 |
| | measured | 80 | 88 | 92 | 94.8 | 76 | 79 | 87.7 | 82 |

**Table 8.** Performance comparison of the proposed antenna with those in the literature.

| Ref. | Antenna type | Frequency band (GHz) | Substrate, Dielectric Constant, Thickness (mm) | Physical size ($W_{sub}\times L_{sub}$) | $-10$ dB Bandwidth (%) | 3 dB ARBW (%) | Gain (dBic) |
|---|---|---|---|---|---|---|---|
| [5] | CRLH-TL | 3.82 | Rogers 5880 $\epsilon_r$= 2.2 $h_{sub}$= 3.175 | $60 \times 60\,\text{mm}^2$ | 0.62 | 0.18 | 6.97 |
| [6] | Patch with meta surface | 3.52 | F4B $\epsilon_r$= 2.65 $h_{sub}$= 2.5 | $40 \times 45\,\text{mm}^2$ | 3.77 | 1.86 | 6.3 |
| [7] | MTM | 3.55 | Teflon, $\epsilon_r$= 2.2 $h_{sub}$= 1.6 | $60 \times 60\,\text{mm}^2$ | 2.53 | 1.42 | 8.2 |
| [8] | (EBG) metasurface | 3.5 | Teflon, $\epsilon_r$= 4.4 $h_{sub}$= 3.2 | $30 \times 30\,\text{mm}^2$ | 34.6 | 6.8 | 3.91 |
| [9] | MTM structures | 4.52 | Teflon, $\epsilon_r$= 2.2 $h_{sub}$= 1.6 | $40 \times 40\,mm^2$ | 3.9 | 2.2 | 1 |
| Proposed Work | Patch with and without shorting pin, meander-line and H-shaped structures | 3.5<br>3.6 | Rogers RO3003 $\epsilon_r$= 3 $h_{sub}$= 1.6 | $25 \times 25\,\text{mm}^2$ | 6.83<br>13.44 | 6.59<br>11.63 | 2.26<br>2.39 |

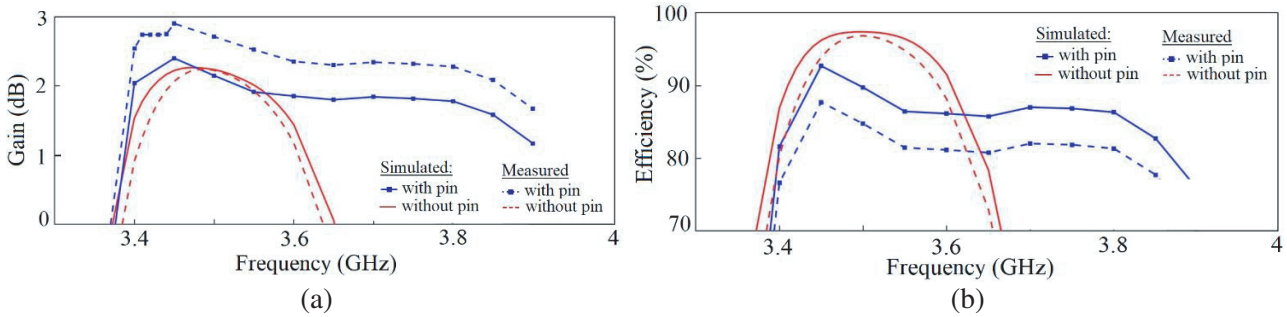


**Figure 11.** Simulated and measured (a) realized gain and (b) efficiency characteristics of the optimal deigned CP antennas without and with shorting pin.

ARBWs are 320 and 200 MHz (510 and 390 MHz). It can be seen from Fig. 11 and Table 7 that there are slight differences between simulated and measured gain and efficiency results for antenna without (with) pin of a maximum difference in gain and efficiency of about 0.27 dB (0.8 dB) and 6% (5%) across the operating frequencies of interest. Thus, an acceptable measured result is obtained which is close to the simulated ones, and the slight difference between them comes from the uncertainty in relative permittivity, heights, and properties of a dielectric material, or inaccuracies in the fabrication and SMA solder processes.

The 2D and 3D far-field gain radiation patterns of the proposed CP antenna without (with) pin at 3.5 GHz (3.6 GHz) are depicted in Fig. 12. The far-field patterns in $E$- and $H$-planes for both antennas as shown in Figs. 12(a) and (b), respectively, demonstrate that they radiate in LHCP in the upper hemisphere and in RHCP in the lower and upper hemispheres. A reasonable similarity is noted in the radiation patterns of two antennas in both $E$-plane and $H$-plane. As Figs. 12(c) and (d) show, 3D radiation patterns like the monopole antenna pattern is exhibited by both antennas with an omnidirectional radiation in the azimuthal ($xz$- or $H$-plane) and a nearly figure of eight in the elevation ($yz$- or $E$-plane). A comparison of the proposed antenna with a few recent works in the literature concerning circularly polarized antennas is summarized in Table 8. It can be observed that the proposed CP antennas have wider ARBW and compact size in comparison with the others.

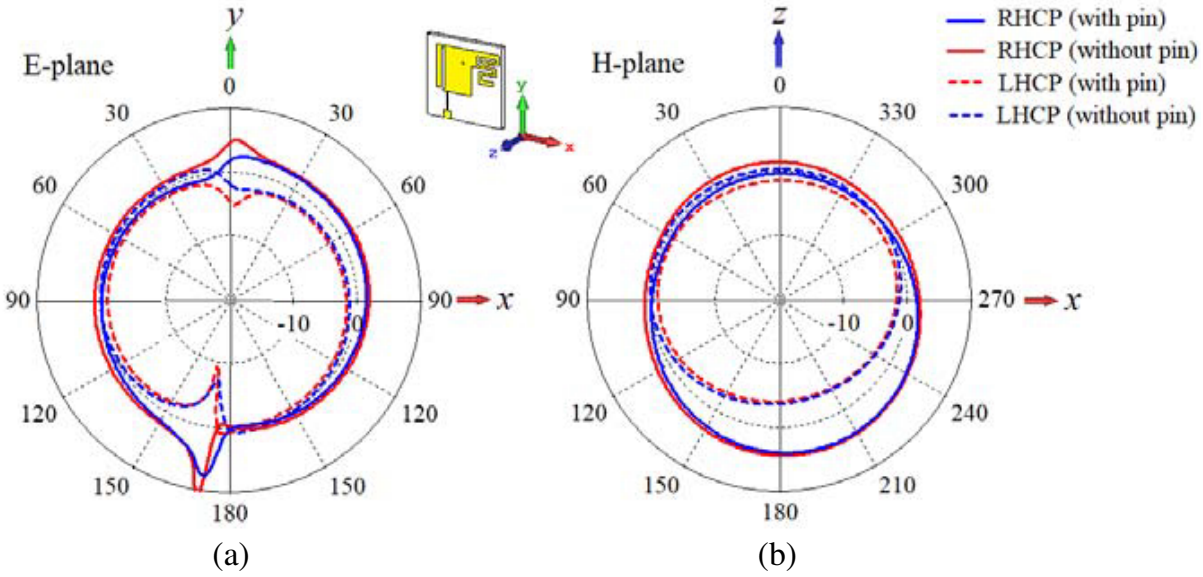

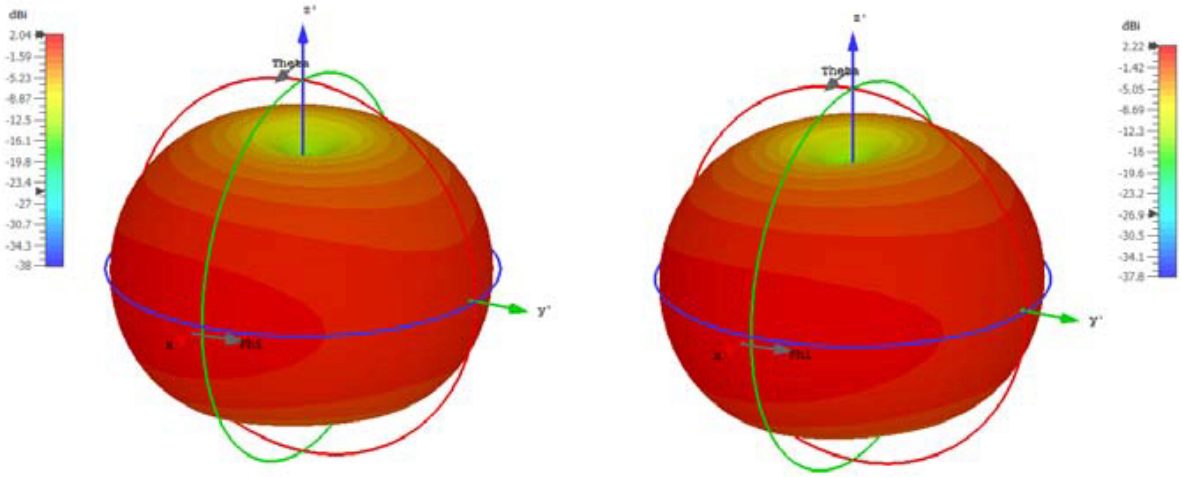

(c) (d)

**Figure 12.** (a) Simulated 2D and 3D realized gain radiation of the CP antenna without (with) shorting pin at 3.5 GHz (3.6 GHz) and (b) $E$-plane and $H$-plane realized gains in polar coordinates. 3D radiation gains for CP antenna (c) with and (d) without pin.

## 6. CONCLUSION

In this work, we have presented an optimization methodology for designing a compact CP antenna which is a promising candidate for LTE bands 42/43 applications. The feature of CP operation is attained by introducing a meander-line and L-shaped strip with an offset line-fed patch radiator printed on a Roger 3003 substrate front layer, and on its back side a rotated H-shaped ground plane is used as a ground plane along with a shorting pin connecting these two layers. The feasible solution of the antenna is obtained by applying a fitness function in the optimization method that combines the PSO algorithm implemented in MATLAB and a powerful CST MWS electromagnetic solver. Two prototypes of the optimized antennas with and without shorting pin having compact size of $25 \times 25\,\text{mm}^2$ are constructed and measured to validate the simulated results which are in reasonably good agreement. The measured results demonstrate that the two antennas (with and without pin) have IBWs for $S_{11} \leq -10\,\text{dB}$ of 220 MHz (3.38–3.6 GHz) and 460 MHz (3.37–3.83 GHz), 3-dB ARBWs of 200 MHz (3.4–3.6 GHz) and 390 MHz (3.42–3.81 GHz) with peak forward RGs of 2.26 and 2.39 dBic, respectively. The proposed CP antenna is suited for LTE 42 (3.4–3.8 GHz) and LTE 43 (3.6–3.8 GHz) band applications. The presented optimization methodology and the proposed fitness function are general and can be applied to design compact antennas of any geometric structures to have CP operation across the desired frequency band.

## REFERENCES


1. Gupta, A. and R. K. Jha, "A survey of 5G network: Architecture and emerging technologies," *IEEE Access*, Vol. 3, 1206–1232, 2015.
2. Arya, A. K., S. J. Kim, S. Park, D.-H. Kim, R. S. Hassan, K. Ko, and S. Kim, "Shark-fin antenna for railway communications in LTE-R, LTE, and lower 5G frequency bands," *Progress In Electromagnetics Research*, Vol. 167, 83–94, 2020.
3. Zhang, L., S. Gao, Q. Luo, P. R. Young, W. Li, and Q. Li, "Inverted-S antenna with wideband circular polarization and wide axial ratio beamwidth," *IEEE Trans. Antennas Propag.*, Vol. 65, No. 4, 1740–1748, Apr. 2017.

4. Beigmohammadi, G., C. Ghobadi, J. Nourinia, and M. Ojaroudi, "Small square slot antenna with circular polarisation characteristics for WLAN/WiMAX applications," *Electronics Letters*, Vol. 46, No. 10, 672–673, 2010.
5. Ko, S. T., B. C. Park, and J. H. Lee, "Dual band circularly polarized patchantenna with first positive and negative modes," *IEEE Antennas Wireless Propag. Lett.*, Vol. 12, 1165–1168, Sept. 2013.
6. Cai, T., G. M. Wang, X. F. Zhang, and J. P. Shi, "Low-profile compact circularly-polarized antenna based on fractal metasurface and fractal resonator," *IEEE Antennas Wireless Propag. Lett.*, Vol. 14, 1072–1076, May 2015.
7. Kuhestani, H., M. Rahimi, and Z. Mansouri, "Dual-band counter circularly polarized radiation from a single-arm metamaterial-based spiral antenna," *Microwave and Optimal Technology Letters*, Vol. 57, 2015.
8. Verma, A., A. K. Singh, and N. Srivastava, "Slot loaded EBG-based metasurface for performance improvement of circularly polarized antenna for WiMAX applications," *International Journal of Microwave and Wireless Technologies*, Vol. 12, No. 3, 1–9, 2019.
9. Cao, W., X. Lv, Z. Zeng, J. Jin, and H. Liu, "Bandwidth enhanced dual-bandpatch-coupling microstrip antenna with omnidirectional CP and unidirectional CP characteristics," *IET Microw. Antennas Propag.*, Vol. 13, No. 5, 584–590, 2019.
10. Tran, H. H., S. X. Ta, and I. Park, "A compact circularly polarized crossed-dipole antenna for an RFID tag," *IEEE Antennas Wireless Propag. Lett.*, Vol. 14, 674–677, Dec. 2014.
11. Lim, S., J. Chen, and C. Cato, "Design of a thin, electrically small, two-element parasitic array with circular polarization," *IEEE Antennas Wireless Propag. Lett.*, Vol. 17, No. 6, 1006–1009, Jun. 2018.
12. Gao, S. S., Q. Luo, and F. Zhu, *Circularly Polarized Antennas*, Wiley, Hoboken, NJ, USA, 2014.
13. Shi, Y. and J. Liu, "A circularly polarized octagon-star-shaped microstrip patch antenna with conical radiation pattern," *IEEE Trans. Antennas Propag.*, Vol. 66, No. 4, 2073–2078, Apr. 2018.
14. Yang, W., Y. Pan, S. Zheng, and P. Hu, "A low-profile wideband circularly polarized crossed-dipole antenna," *IEEE Antennas Wireless Propag. Lett.*, Vol. 16, 2126–2129, May 2017.
15. Yang, H. C., X. Y. Liu, Y. Fan, and M. M. Tentzeris, "Flexible circularly polarized antenna with axial ratio bandwidth enhancement for off-body communications," *IET Microw. Antennas Propag.*, Vol. 15, 754–767, 2021.
16. Le, T. T., H. H. Tran, and A. A. Althuwayb, "Wideband circularly polarized antenna based on a non-uniform metasurface," *Applied Sciences*, Vol. 10, No. 23, 8652, 2020.
17. Guo, Y.-X. and D. C. H. Tan, "Wideband single-feed circularly polarized patch antenna withconical radiation pattern," *IEEE Antennas Wireless Propag. Lett.*, Vol. 8, 924–926, Jul. 2009.
18. Zhang, H., Y. Guo, and G. Wang, "A wideband circularly polarized crossed-slot antenna with stable phase center," *IEEE Antennas Wireless Propag. Lett.*, Vol. 18, No. 5, 941–945, May 2019.
19. Yaseen, R. M., D. K. Naji, and A. M. Shakir, "Optimization design methodology of broadband or multiband antenna for RF energy harvesting applications," *Progress In Electromagnetics Research B*, Vol. 93, 169–194, 2021.
20. Boursianis, D., et al., "Multiband patch antenna design using nature-inspired optimization method," *IEEE Open Journal of Antennas and Propagation*, Vol. 2, 151–162, 2021.
21. Jabar, A. A. S. A. and D. K. Naji, "Optimization design methodology of miniaturized five-band antenna for RFID, GSM, and WiMAX applications," *Progress In Electromagnetics Research B*, Vol. 83, 177–201, 2019.
22. Moore, M., Z. Iqbal, and S. Lim, "A size-reduced, broadband, bidirectional, circularly polarized antenna for potential application in WLAN, WiMAX, 4G, and 5G frequency bands," *Progress In Electromagnetics Research C*, Vol. 114, 1–11, 2021.
23. Pietrenko-Dabrowska, A. and S. Koziel, "Expedited antenna optimization with numerical derivatives and gradient change tracking," *Engineering Computations*, Vol. 37, No. 4, 1179–1193, 2020.
24. Balanis, C. A., *Antenna Theory Analysis and Design*, 4th Edition, John Wiley & Sons, 2016.